ChemComm

COMMUNICATION

View Article Online
View Journal | View Issue

Cite this: *Chem. Commun.*, 2024, **60**, 3681

Received 13th January 2024,
Accepted 29th February 2024

DOI: 10.1039/d4cc00186a

rsc.li/chemcomm

Formation of paired Ga sites in CHA-type zeolite frameworks *via* a transcription-induced method†

Takumi Kaneko,[a] Mizuho Yabushita,*[a] Ryota Osuga,[b] Yugo Sawada,[a] Kei Sato,[a] Ben Liu,[a] Yoshinao Nakagawa,[a] Kiyotaka Nakajima[b] and Keiichi Tomishige*[ac]

Paired Ga sites represented by the Ga–O–Si–O–Ga sequence were firstly formed intentionally in CHA-type zeolite frameworks *via* the transcription of pre-formed paired Ga species in a Ga-rich amorphous silica–gallia under seed-assisted hydrothermal conditions. Such paired Ga sites behaved as ion-exchange sites for capturing divalent cation, Co^{2+}.

Control of location and distribution of isomorphously substituting trivalent heteroatoms (*e.g.*, Al^{3+} and Ga^{3+}) is the key to tuning various characteristics of porous and crystalline metallosilicates (*i.e.*, zeolites), such as acidic properties, thermal stability, catalytic performance, and ion-exchange properties.[1] The isomorphous substitution of trivalent heteroatoms into zeolite frameworks generates ion-exchange sites in a one-to-one correspondence for charge compensation. Because isomorphously substituting heteroatoms are typically isolated from each other in zeolite frameworks, ion-exchange sites on such heteroatoms capture monovalent cations. Meanwhile, the demand for capturing divalent cations by zeolite frameworks has grown due to the desire for preparing highly active catalysts where divalent cationic species serve as active sites[1e,2] and also removing harmful heavy-metal cations that are typically multivalent from water.[3] For such demand, two trivalent heteroatoms need to be placed intentionally in zeolite frameworks in close proximity, yet the formation of the nearest neighboring pair represented by the M–O–M sequence (M = heteroatom) in zeolite frameworks is impossible due to the violation of Loewenstein's rule.[4] Instead of such unrealizable species, the formation of the second nearest neighboring pairs (so-called paired M sites) represented by the M–O–Si–O–M sequence has thus been targeted in the field of zeolite chemistry.[1b–e,5] The increase of heteroatom content in zeolite frameworks is the simplest means of forming paired M sites due to the enhanced probability of juxtaposition of two heteroatoms, but this means cannot be easily applied to high-silica zeolites (Si/M molar ratio $\geq$ 5). The development of a well-designed approach for the formation of paired M sites even in high-silica zeolite frameworks is, therefore, necessary.

A variety of synthetic strategies have been reported for the formation of paired Al sites in zeolite frameworks thus far (Table S1, ESI†). The sources of Si and Al were found to be important for the formation of paired Al sites in high-silica **MFI**-type frameworks.[6] The synthetic strategy reported by Gounder *et al.* relied on the static interaction between positively-charged structure-directing agents (SDAs) and negatively-charged building blocks containing paired Al species.[7] The combination of a bulky *N*,*N*,*N*-trimethyl-1-adamantylammonium cation ($TMAda^+$) and small Na^+ enabled the simultaneous compensation against two negative charges of the building blocks and construction of high-silica **CHA**-type zeolites with paired Al sites. The different synthetic concept reported by Yokoi *et al.* was the transcription of paired Al sites from **FAU**-type to **CHA**-type zeolite during the interzeolite conversion.[8] The key of their procedure was the use of **FAU**-type zeolite with the low Si/Al ratio of 2.4–2.8, where the content of paired Al sites was enriched by the enhancement of the juxtaposition probability. We reported the transcription of paired Al sites from the Al-rich amorphous silica–alumina (Si/Al = 2.5) into the **CHA**- and **MFI**-type zeolite frameworks along with the controlled content of paired Al sites.[9] These reports on the "transcription-induced method" are the first examples of the intentional formation of paired Al sites in multiple framework types *via* the same strategy. The uniqueness of this method arises from the use of amorphous Si–Al mixed oxide as a precursor. Although the use of zeolites as precursors (*i.e.*, interzeolite conversion) limits the scope of framework types because of the proposed requirement of the structural similarity between the

[a] *Department of Applied Chemistry, School of Engineering, Tohoku University, 6-6-07 Aoba, Aramaki, Aoba-ku, Sendai, Miyagi 980-8579, Japan. E-mail: m.yabushita@tohoku.ac.jp, tomishige@tohoku.ac.jp*
[b] *Institute for Catalysis, Hokkaido University, Kita 21 Nishi 10, Kita-ku, Sapporo, Hokkaido 001-0021, Japan*
[c] *Advanced Institute for Materials Research (WPI-AIMR), Tohoku University, 2-1-1 Katahira, Aoba-ku, Sendai, Miyagi 980-8577, Japan*

† Electronic supplementary information (ESI) available: Experimental, summary of related works, and characterization data. See DOI: https://doi.org/10.1039/d4cc00186a

parent and daughter zeolites,[10] such a limitation can be omitted in the case of an amorphous precursor. All the approaches introduced here succeeded in the formation of paired sites consisting of Al atoms in zeolite frameworks; however, the construction of paired sites composed of other heteroatoms such as Ga has not yet been reported thus far. According to previous reports, the affinity between protons and negatively charged zeolite frameworks is dependent on a class of isomorphous substituting heteroatoms,[11] positing that the affinity of divalent cations with paired sites is governed by such heteroatoms; this insight has also boosted our motivation to intentionally create paired Ga sites in zeolite frameworks. The achievements of the aforementioned transcription-induced method suggested that if paired heteroatom species are prepared in an amorphous Si-containing mixed oxide by enriching the content of desired heteroatoms, such species can be transcribed into zeolite frameworks. Based on this hypothesis, in this manuscript, the transcription-induced method was applied to the formation of paired Ga sites in zeolite frameworks. A **CHA**-type framework was targeted here since this framework possesses single crystallographically distinct tetrahedral sites (T-sites) and thus offers the ease of structural characterization and understanding.

The precursor of the zeolites (*i.e.*, Ga-rich silica–gallia) was prepared *via* the Pechini method.[12] The detailed procedure is summarized in the Experimental section and Fig. S1 (ESI†). The molar ratio of Si/Ga in the prepared sample was determined by ICP-OES to be 1.9, which was almost identical to the value based on the charged sources of Si and Ga (Si/Ga = 2.0). In its XRD pattern (Fig. S2A, ESI†), the halo at *ca.* 22° characteristic of amorphous materials and the broad peaks attributable to β-Ga_2O_3 were observed, indicating that the most part of this material was amorphous, yet some amount of β-Ga_2O_3 was also involved. This material had a stone-like shape with the size of *ca.* 100–200 nm (Fig. S2B, ESI†). In the ^{71}Ga MAS NMR spectrum (Fig. S2C, ESI†), two peaks at 34 and 133 ppm assignable to octahedral and tetrahedral Ga species, respectively,[13] were observed. The difference in their intensity suggested the dominant Ga species to be octahedral ones. The broad signal in the range of −125 to −85 ppm in the ^{29}Si MAS NMR spectrum (Fig. S2D, ESI†) indicated the presence of $Q^4(n\mathrm{Ga})$ ($0 \le n \le 4$; $Si(OSi)_{4-n}(OGa)_n$; Q^4(2Ga) corresponds to paired Ga sites), similar to the previous case of Al-rich silica–alumina.[9] The absence of signals in the ^{29}Si CP/MAS NMR spectrum in Fig. S2D (ESI†) suggested that the content of defect sites represented by $Si(OT)_{4-m}(OH)_m$ (T = Si or Ga, $1 \le m \le 3$) was negligible.

The seed-assisted hydrothermal treatment for the thus-prepared Ga-rich silica–gallia was conducted with $TMAda^+$ and Na^+ at different durations to synthesize [Ga]-CHA-t_2 samples (t_2 is the aging time after adding the Ga-rich silica–gallia into each synthesis gel; see Experimental and Fig. S1, ESI†). In these tests, t_2 was kept constant at 9 h. The data of relative crystallinity, solid yield, and characterization indicated that the crystallization proceeded rapidly between the hydrothermal treatment time of 4–5 h and also that 72 h was the optimum duration for synthesizing [Ga]-CHA-t_2 (Fig. S3–S6 and Table S2; the detailed discussion is available in ESI†). We should note that the hydrothermal treatment of tetraethyl orthosilicate and $Ga(NO_3)_3$ under the same conditions failed to yield a **CHA**-type framework, demonstrating that the use of the Ga-rich silica–gallia is the key to the construction of the **CHA**-type framework.

Under the optimum duration of hydrothermal treatment (*i.e.*, 72 h), a series of [Ga]-CHA-t_2 samples were synthesized by altering the aging time t_2 from 0 h to 24 h, since this parameter was previously found as the key to controlling the proportion of paired Al sites.[9] The solid yields and Si/Ga molar ratios were almost constant at 67–70% and 5.5–5.7, respectively (Table 1). The latter values were lower than those of each synthesis gel (*i.e.*, 10) possibly because some amount of Si species remained dissolved in the solution. All the [Ga]-CHA-t_2 samples were revealed by XRD to possess the **CHA**-type architecture (Fig. 1). The crystalline particles were also confirmed from their SEM images (Fig. S7, ESI†). The textural properties of these [Ga]-CHA-t_2 samples were examined by N_2 physisorption measurement (Fig. S8, ESI†). The type-I isotherms were observed for all the samples, indicating their microporous environment given by the zeolite framework. Both the BET surface area (594–711 $m^2\ g^{-1}$) and total pore volume

Table 1 Textual properties and Co^{2+} exchange performance of [Ga]-CHA-t_2 samples

Sample	Solid yield/%	Si/Ga ratio	S_{BET}[a]/ $m^2\ g^{-1}$	V_{total}[b]/ $cm^3\ g^{-1}$	Proportion of $Q^4(n\mathrm{Ga})$[c]/%			Proportion of Ga-containing $Q^4(n\mathrm{Ga})$[d]/%		Co^{2+} uptake/ mg g_{CHA}^{-1}	2Co/ Ga ratio
					Q^4(0Ga)	Q^4(1Ga)	Q^4(2Ga)	Q^4(1Ga)	Q^4(2Ga)		
[Ga]-CHA-0	68	5.5	658	0.34	64 ± 2	32 ± 1	3.7 ± 0.1	90 ± 3	10 ± 0	26	0.46
[Ga]-CHA-3	68	5.5	663	0.33	58 ± 1	36 ± 1	5.5 ± 0.2	87 ± 2	13 ± 0	29	0.50
[Ga]-CHA-6	70	5.5	678	0.34	62 ± 1	32 ± 1	6.2 ± 0.2	84 ± 2	16 ± 1	33	0.56
[Ga]-CHA-9	69	5.7	711	0.31	59 ± 1	33 ± 1	7.9 ± 0.2	81 ± 2	19 ± 1	34	0.60
[Ga]-CHA-12	67	5.5	599	0.30	58 ± 1	36 ± 1	6.7 ± 0.2	84 ± 2	16 ± 0	35	0.60
[Ga]-CHA-24	68	5.5	594	0.30	57 ± 1	37 ± 1	6.1 ± 0.2	86 ± 2	14 ± 0	33	0.56

[a] BET specific surface area. [b] Total pore volume. [c] Estimated from the areas of each $Q^4(n\mathrm{Ga})$ peak in the ^{29}Si MAS NMR spectra (Fig. S9B and S10, ESI): (proportion of $Q^4(n\mathrm{Ga})$ (n = 0–2)) = (peak area for $Q^4(n\mathrm{Ga})$)/((peak area for Q^4(0Ga)) + (peak area for Q^4(1Ga)) + (peak area for Q^4(2Ga))). [d] Estimated from the areas of each $Q^4(n\mathrm{Ga})$ peak in the ^{29}Si MAS NMR spectra (Fig. S9B and S10, ESI): (proportion of Ga-containing $Q^4(n\mathrm{Ga})$ (n = 1 or 2)) = (peak area for $Q^4(n\mathrm{Ga})$)/((peak area for Q^4(1Ga)) + (peak area for Q^4(2Ga))).

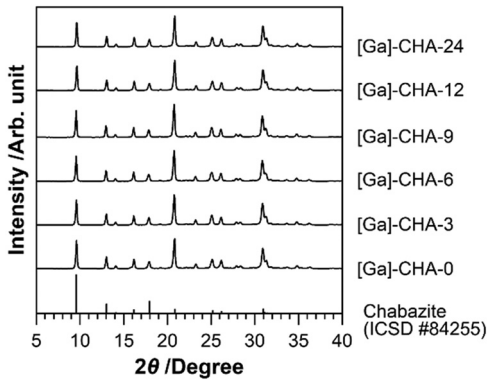

Fig. 1 XRD patterns of [Ga]-CHA-t_2 synthesized at different aging times (t_2 = 0–24 h).

(0.30–0.34 $cm^3\ g^{-1}$) determined from these isotherms indicated the sufficient quality of our synthesized samples (Table 1), due to their similarity to reported values.[7a,c,8a,9a]

Fig. S9A (ESI†) shows the ^{71}Ga MAS NMR spectra of the [Ga]-CHA-t_2 samples. In these spectra, only the peak at 168 ppm assignable to tetrahedral Ga species[14] was observed with no observable peak at *ca.* 0 ppm, indicating that the Ga species in these samples were incorporated into the framework. In the ^{29}Si MAS NMR spectra in Fig. S9B (ESI†), there are three peaks at −111, −103, and −95 ppm, which are assignable to Q^4(0Ga), Q^4(1Ga), and Q^4(2Ga), respectively.[15] Meanwhile, no peaks were seen in the ^{29}Si CP/MAS NMR spectra (Fig. S9C, ESI†), indicating the negligible amount of defect sites in all the [Ga]-CHA-t_2 samples and allowing the estimation of the proportion of Q^4(nGa) peaks in the ^{29}Si MAS NMR spectra. The curve fitting for the ^{29}Si MAS NMR spectra in Fig. S10 (ESI†) provided the proportion of the three Q^4(nGa) peaks (Table 1). The proportion of Q^4(2Ga) in the Ga-containing Q^4(nGa) (n = 1 or 2) gradually increased from 10 to 19% as the aging time t_2 increased from 0 to 9 h, while it decreased to 14% by further extension of t_2 to 24 h. This trend is consistent with the previous cases of construction of paired Al sites *via* the same approach.[9] Such volcano-type dependence of the proportion of Q^4(2Ga) as a function of t_2 can be rationalized by the same reason invoked previously.[9] The short aging ($t_2 < 9$ h) was insufficient for supplying suitable building blocks containing paired Ga species from the precursor *via* its hydrolysis and dissolution caused by bases (TMAdaOH and NaOH). Meanwhile, the longer aging ($t_2 > 9$ h) triggered the degradation of such building blocks to lose the pre-formed paired Ga species. This is the first example to intentionally create paired Ga sites with the control of their contents in any type of zeolite frameworks.

In addition to the acidic character of the thus-prepared paired Ga sites in the [Ga]-CHA-t_2 samples (the TPD data (Fig. S11 and Table S3) and discussion are available in the ESI†), the performance of the thus-prepared paired Ga sites in [Ga]-CHA-t_2 as ion-exchange sites for capturing divalent cations was evaluated with Co^{2+} as a probe ion, which was also used in previous reports.[9b,16] Table 1 lists the Co^{2+} uptake determined after ion-exchange treatment followed by ICP-OES. The Co^{2+} uptake showed the volcano-type dependence as a function of t_2 with the maximum value at around 9–12 h. This trend is similar to that of the proportion of Q^4(2Ga) examined by ^{29}Si MAS NMR (*vide supra*), indicating that the paired Ga sites formed in [Ga]-CHA-t_2 functioned as ion-exchange sites for Co^{2+}. The 2Co/Ga molar ratios were calculated to be at most 0.60 (Table 1), the value of which was comparable to or even higher than the molar ratios of the divalent cation (Co^{2+} or Sr^{2+}) to isomorphously substituted Al in previous works (Table S1, ESI†).[6,7,9] If all Ga atoms participated in the formation of paired Ga sites and all pair sites successfully captured Co^{2+}, the 2Co/Ga molar ratio should become 1.0. The difference between the experimentally-observed values and this ideal one suggested two possibilities for the [Ga]-CHA-t_2 samples: (i) some of the intraframework Ga species are present as isolated species and/or (ii) some of the paired Ga species cannot function as ion-exchange sites for capturing Co^{2+} probably due to the limited space in the **CHA**-type framework. For more detail about the latter case, if two paired Ga sites are in close proximity, one of two Co^{2+} cations cannot be introduced due to the steric effect given by another Co^{2+} successfully introduced on the paired Ga sites.

The Co^{2+} species introduced on the [Ga]-CHA-t_2 samples were further characterized by DR-UV-vis spectroscopy and XAS. In the DR-UV-vis spectra (Fig. S12A, ESI†), prominent absorption bands were observed with their maxima at 19 400 and ~43 000 cm^{-1} for all the samples. The former band was attributed to d–d transitions of Co^{2+} species anchored on paired sites.[9b,16] According to previous literature, the latter band is assignable to ligand-to-metal charge transfer from intraframework oxygen atoms to Co^{2+},[9b,17] while the intensity of this peak is known to be weakened upon dehydrating treatment at high temperature *in vacuo*.[16a,18] These reports suggest that the Co^{2+} species introduced on the [Ga]-CHA-t_2 samples were hydrated to some extent due to a lack of dehydrating treatment in this study (see Experimental). The Co K-edge XANES spectra of the Co^{2+}-exchanged [Ga]-CHA-t_2 samples confirmed the valence of Co species as +2 due to the consistency of the absorption edge energy of these samples with that of CoO (Fig. S12B, ESI†). Besides, although the pre-edge peak was observed for all the Co^{2+}-exchanged [Ga]-CHA-t_2 samples, its intensity was low and close to that of CoO (Fig. S12C, ESI†). This observation suggested the presence of octahedrally coordinated Co^{2+} species rather than tetrahedrally coordinated ones, the latter of which provides a prominent pre-edge peak like the case of Co_3O_4. The curve-fitting results for the Co K-edge EXAFS oscillation (Fig. S13, ESI†) are summarized in Table 2. The oscillations for all the samples were fitted well with the sole shell of Co–O, and the coordination number (CN) for this shell was estimated to be *ca.* 5–6. Considering the Co^{2+} species anchored on the paired Ga sites (*i.e.*, four coordination) as well as the presence of hydrating water molecules as indicated by the DR-UV-vis spectra (*vide supra*), these CN values suggested that one or two water molecules were present at each Co^{2+} species on average. Such insight into the coordination of Co^{2+} is in good agreement with the indication by XANES

Table 2 Curve fitting results for Co K-edge EXAFS data of Co^{2+}-exchanged [Ga]-CHA-t_2 samples[a]

Sample	Shell	CN[b]	$R^c/10^{-1}$ nm	$\sigma^d/10^{-1}$ nm	$\Delta E_0{}^e$/eV	$R_f{}^f$/%	FF range[g]/nm–nm
Co^{2+}/[Ga]-CHA-0	Co–O	5.8 ± 0.8	2.08 ± 0.01	0.085 ± 0.009	−2.2 ± 1.5	1.8	0.952–2.117
Co^{2+}/[Ga]-CHA-3	Co–O	4.9 ± 0.4	2.06 ± 0.01	0.083 ± 0.006	−4.2 ± 1.1	0.80	0.952–2.117
Co^{2+}/[Ga]-CHA-6	Co–O	4.9 ± 0.4	2.06 ± 0.01	0.075 ± 0.005	−5.0 ± 0.9	0.54	0.952–2.117
Co^{2+}/[Ga]-CHA-9	Co–O	5.2 ± 0.3	2.06 ± 0.00	0.079 ± 0.004	−3.6 ± 0.6	0.25	0.952–2.117
Co^{2+}/[Ga]-CHA-12	Co–O	5.1 ± 0.3	2.06 ± 0.01	0.081 ± 0.004	−3.9 ± 0.7	0.34	0.952–2.117
Co^{2+}/[Ga]-CHA-24	Co–O	5.4 ± 0.4	2.07 ± 0.01	0.083 ± 0.005	−2.5 ± 0.9	0.67	0.952–2.117

[a] EXAFS data are shown in Fig. S13 (ESI). [b] Coordination number. [c] Bond distance. [d] Debye–Waller factor. [e] Difference in the origin of photoelectron energy between the reference and the sample. [f] Residual factor. [g] Fourier-filtering range.

(*i.e.*, the presence of octahedrally coordinated Co^{2+} species). Meanwhile, a fingerprint FT-EXAFS peak assignable to M′–O–T (M′ = metal cation introduced *via* ion exchange; T = Si or isomorphously substituting heteroatom), which typically has a bond length of *ca.* 0.23 nm,[19] was not observed clearly (Fig. S13, ESI†). Such unclearness in the current FT-EXAFS data is possibly due to thermal fluctuation. Altogether, these spectroscopic data stressed the function of paired Ga sites formed in [Ga]-CHA-t_2 as ion-exchange sites for divalent cation, Co^{2+}.

In conclusion, the transcription-induced method was applied to the formation of paired Ga sites in the **CHA**-type zeolite frameworks. The paired Ga species were pre-formed in the Ga-rich amorphous silica–gallia *via* the Pechini method and subsequently transcribed from this amorphous precursor into the **CHA**-type frameworks during the hydrothermal process. The key synthetic parameter for controlling the proportion of paired Ga sites elucidated as Q^4(2Ga) species by ^{29}Si MAS NMR spectroscopy was the aging time after the addition of the Ga-rich amorphous silica–gallia into a synthesis gel (*i.e.*, t_2). The intermediate aging time of 9 h was found to maximize the proportion of paired Ga sites, and the shorter and longer aging time decreased the paired Ga sites. The [Ga]-CHA-t_2 sample with the higher proportion of Q^4(2Ga) species exhibited higher Co^{2+} uptake, suggesting that the paired Ga species in [Ga]-CHA-t_2 functioned correctly as ion-exchange sites for divalent cations. These data posited the potential of zeolites with paired sites for purifying water contaminated by toxic divalent metal cations (*e.g.*, ^{60}Co is a radioactive and hazardous isotope). The transcription-induced method thus has the potential to be a universal means of creating paired sites consisting of Ga and Al in various types of zeolite frameworks and open the door to further precise design of zeolite-based functional materials.

This work was supported financially by the following grants: JSPS KAKENHI (21H05011, 23K04494, and 23K20034); the Japan Petroleum Institute; the Kurita Water and Environment Foundation (21A023, 22K002, and 23K002); and the Joint Usage/Research Center for Catalysis (22AY0062 and 23AY0301). B. L. acknowledges the JST fellowship (JPMJFS2102).

Conflicts of interest

There are no conflicts to declare.

References

1 (*a*) J. Čejka, A. Corma and S. Zones, *Zeolites and catalysis: synthesis, reactions and applications*, Wiley-VCH, Weinheim, 2010; (*b*) M. Yabushita, R. Osuga and A. Muramatsu, *CrystEngComm*, 2021, **23**, 6226–6233; (*c*) J. Bae and M. Dusselier, *Chem. Commun.*, 2023, **59**, 852–867; (*d*) J. Li, M. Gao, W. Yan and J. Yu, *Chem. Sci.*, 2023, **14**, 1935–1959; (*e*) M. Yabushita, R. Osuga, T. Yokoi and A. Muramatsu, *Catal. Sci. Technol.*, 2023, **13**, 4020–4044.
2 (*a*) E. Borfecchia, P. Beato, S. Svelle, U. Olsbye, C. Lamberti and S. Bordiga, *Chem. Soc. Rev.*, 2018, **47**, 8097–8133; (*b*) M. A. Newton, A. J. Knorpp, V. L. Sushkevich, D. Palagin and J. A. van Bokhoven, *Chem. Soc. Rev.*, 2020, **49**, 1449–1486.
3 (*a*) G. Blanchard, M. Maunaye and G. Martin, *Water Res.*, 1984, **18**, 1501–1507; (*b*) M. Hua, S. Zhang, B. Pan, W. Zhang, L. Lv and Q. Zhang, *J. Hazard. Mater.*, 2012, **211–212**, 317–331.
4 W. Loewenstein, *Am. Mineral.*, 1954, **39**, 92–96.
5 J. Dědeček, Z. Sobalík and B. Wichterlová, *Catal. Rev.*, 2012, **54**, 135–223.
6 (*a*) V. Gábová, J. Dědeček and J. Čejka, *Chem. Commun.*, 2003, 1196–1197; (*b*) J. Dedecek, V. Balgová, V. Pashkova, P. Klein and B. Wichterlová, *Chem. Mater.*, 2012, **24**, 3231–3239.
7 (*a*) J. R. Di Iorio and R. Gounder, *Chem. Mater.*, 2016, **28**, 2236–2247; (*b*) J. R. Di Iorio, S. Li, C. B. Jones, C. T. Nimlos, Y. Wang, E. Kunkes, V. Vattipalli, S. Prasad, A. Moini, W. F. Schneider and R. Gounder, *J. Am. Chem. Soc.*, 2020, **142**, 4807–4819; (*c*) P. M. Kester, J. T. Crum, S. Li, W. F. Schneider and R. Gounder, *J. Catal.*, 2021, **395**, 210–226.
8 (*a*) T. Nishitoba, N. Yoshida, J. N. Kondo and T. Yokoi, *Ind. Eng. Chem. Res.*, 2018, **57**, 3914–3922; (*b*) T. Nishitoba, T. Nozaki, S. Park, Y. Wang, J. N. Kondo, H. Gies and T. Yokoi, *Catalysts*, 2020, **10**, 1204.
9 (*a*) M. Yabushita, Y. Imanishi, T. Xiao, R. Osuga, T. Nishitoba, S. Maki, K. Kanie, W. Cao, T. Yokoi and A. Muramatsu, *Chem. Commun.*, 2021, **57**, 13301–13304; (*b*) Y. Imanishi, R. Osuga, A. Muramatsu and M. Yabushita, *J. Jpn. Pet. Inst.*, 2023, **66**, 246–253.
10 (*a*) T. Sano, M. Itakura and M. Sadakane, *J. Jpn. Pet. Inst.*, 2013, **56**, 183–197; (*b*) J. Devos, M. A. Shah and M. Dusselier, *RSC Adv.*, 2021, **11**, 26188–26210.
11 C. T. W. Chu and C. D. Chang, *J. Phys. Chem.*, 1985, **89**, 1569–1571.
12 (*a*) J. Dědeček and B. Wichterlová, *J. Phys. Chem. B*, 1999, **103**, 1462–1476; (*b*) D. Kaucký, J. Dědeček and B. Wichterlová, *Microporous Mesoporous Mater.*, 1999, **31**, 75–87.
13 M. P. Pechini, *US Pat.*, 3330697A, 1967.
14 J. T. Ash and P. J. Grandinetti, *Magn. Reson. Chem.*, 2006, **44**, 823–831.
15 A. P. M. Kentgens, C. R. Bayense, J. H. C. van Hooff, J. W. de Haan and L. J. M. van de Ven, *Chem. Phys. Lett.*, 1991, **176**, 399–403.
16 N. Janes and E. Oldfield, *J. Am. Chem. Soc.*, 1985, **107**, 6769–6775.
17 M. Bernauer, E. Tabor, V. Pashkova, D. Kaucký, Z. Sobalík, B. Wichterlová and J. Dedecek, *J. Catal.*, 2016, **344**, 157–172.
18 J. D. Han and S. I. Woo, *Korean J. Chem. Eng.*, 1991, **8**, 235–239.
19 (*a*) K. A. Lomachenko, E. Borfecchia, C. Negri, G. Berlier, C. Lamberti, P. Beato, H. Falsig and S. Bordiga, *J. Am. Chem. Soc.*, 2016, **138**, 12025–12028; (*b*) V. L. Sushkevich, O. V. Safonova, D. Palagin, M. A. Newton and J. A. van Bokhoven, *Chem. Sci.*, 2020, **11**, 5299–5312.

